University of Nebraska - Lincoln
DigitalCommons@University of Nebraska - Lincoln

Ralph Skomski Publications | Research Papers in Physics and Astronomy

2013

Magnetism and electron transport of MnyGa (1 < y < 2) nanostructures

Yung Huh
University of Nebraska-Lincoln, yung.huh@sdstate.edu

Parashu Kharel
University of Nebraska-Lincoln, pkharel2@unl.edu

Shah R. Valloppilly
University of Nebraska-Lincoln, svalloppilly2@unl.edu

XINGZHONG LI
Nebraska Center for Materials and Nanoscience, xli2@unl.edu

Ralph Skomski
University of Nebraska-Lincoln, rskomski2@unl.edu

See next page for additional authors

Follow this and additional works at: https://digitalcommons.unl.edu/physicsskomski

Huh, Yung; Kharel, Parashu; Valloppilly, Shah R.; LI, XINGZHONG; Skomski, Ralph; and Sellmyer, David J., "Magnetism and electron transport of MnyGa (1 < y < 2) nanostructures" (2013). *Ralph Skomski Publications*. 83.
https://digitalcommons.unl.edu/physicsskomski/83

This Article is brought to you for free and open access by the Research Papers in Physics and Astronomy at DigitalCommons@University of Nebraska - Lincoln. It has been accepted for inclusion in Ralph Skomski Publications by an authorized administrator of DigitalCommons@University of Nebraska - Lincoln.

Authors

Yung Huh, Parashu Kharel, Shah R. Valloppilly, XINGZHONG LI, Ralph Skomski, and David J. Sellmyer

This article is available at DigitalCommons@University of Nebraska - Lincoln: https://digitalcommons.unl.edu/physicsskomski/83

Magnetism and electron transport of Mn_yGa ($1 < y < 2$) nanostructures

Y. Huh,[1,2] P. Kharel,[1,3] V. R. Shah,[1] X. Z. Li,[1] R. Skomski,[1,3] and D. J. Sellmyer[1,3]
[1]*Nebraska Center for Materials and Nanoscience, University of Nebraska, Lincoln, Nebraska 68588, USA*
[2]*Department of Physics, South Dakota State University, Brookings, South Dakota 57007, USA*
[3]*Department of Physics and Astronomy, University of Nebraska, Lincoln, Nebraska 68588, USA*

(Received 24 April 2013; accepted 13 June 2013; published online 1 July 2013)

Nanostructured Mn_yGa ribbons with varying Mn concentrations including $Mn_{1.2}Ga$, $Mn_{1.4}Ga$, $Mn_{1.6}Ga$, and $Mn_{1.9}Ga$ were prepared using arc-melting and melt-spinning followed by a heat treatment. Our experimental investigation of the nanostructured ribbons shows that the material with $y = 1.2$, 1.4, and 1.6 prefers the tetragonal $L1_0$ structure and that with $y = 1.9$ prefers the $D0_{22}$ structure. We have found a maximum saturation magnetization of 621 emu/cm^3 in $Mn_{1.2}Ga$ which decreases monotonically to 300 emu/cm^3 as y reaches 1.9. Although both the $L1_0$- and $D0_{22}$-Mn_yGa samples show a high Curie temperature (T_c) well above room temperature, the value of T_c decreases almost linearly from 702 K for $Mn_{1.9}Ga$ to 551 K for $Mn_{1.2}Ga$. All the ribbons are metallic between 2 K and 300 K but the $Mn_{1.2}Ga$ also shows a resistance minimum near 15 K. The observed magnetic properties of the Mn_yGa ribbons are consistent with the competing ferromagnetic coupling between Mn moments in the regular $L1_0$-MnGa lattice sites and antiferromagnetic coupling with excess Mn moments occupying Ga sites. © *2013 AIP Publishing LLC*. [http://dx.doi.org/10.1063/1.4812561]

INTRODUCTION

Magnetic materials having high magnetic anisotropy and Curie temperature well above room temperature have high potential for a range of applications including high-density recording, nonvolatile memory, and permanent-magnet materials.[1–3] Most high-anisotropy magnets contain either rare-earth elements or noble metals such as Pt.[3] Some of the rare-earth elements used in strong permanent magnets are critical materials and there are serious concerns over the price and supply of these materials.[4] Therefore, there have been intense research efforts in identifying and developing novel rare-earth free high-anisotropy magnets. Some of the non-rare-earth-element-based permanent magnet materials of current interest are the manganese-based ferromagnetic materials including MnBi,[5,6] MnAl,[7] and MnGa.[8–10] Among these three magnets, Mn_yGa is particularly interesting because its magnetic properties can be tuned by varying y to fit specific magnetic and magnetoelectronic applications.[11,12]

Mn_yGa can be synthesized in multiple crystallographic structures including cubic (disordered Cu_3Au-type structure), hexagonal ($D0_{19}$), tetragonal ($L1_0$), and tetragonal ($D0_{22}$) structures.[13] Theoretically, Mn_3Ga in a cubic Heusler ($L2_1$) structure with half-metallic electronic band structure has also been predicted but there is no experimental evidence to support this prediction to date.[14] The most extensively studied phases of Mn_yGa compounds are the tetragonal $L1_0$ ($1 < y < 1.8$) and $D0_{22}$ ($2 \le y \le 3$) structures. Theoretically, Mn_yGa compounds in $L1_0$ and $D0_{22}$ structures are expected to have anisotropy constant K_u of 26 and 20 Mergs/cm^3, magnetization M_s of 845 and 305 emu/cm^3, energy product $(BH)_{max}$ of 28.2 and 3.67 MGOe, and spin polarization at the Fermi level of 71% and 88%, respectively.[15,16] The highest experimental values of H_c and K_u for $L1_0$-Mn_yGa are reported for $L1_0$-$Mn_{1.5}Ga$ films grown epitaxially on GaAs substrates and are 42.8 kOe and 21.7 Mergs/cm^3, respectively.[9] Although $L1_0$-Mn_yGa shows relatively small magnetization for permanent-magnet application, the high values of anisotropy constant and coercivity; and Curie temperature well above room temperature are promising and the material might be used to develop nanocomposite permanent magnets. Therefore, it is important to understand the structural and magnetic properties of $L1_0$-Mn_yGa compound in nanoparticle or nanoribbon form. Further, the predicted high value of spin polarization (71%) has motivated us to investigate its electrical properties as well. Here, we present our experimental investigation on the structural, magnetic, and electron-transport properties of single phase $L1_0$-Mn_yGa ($y = 1.2$, 1.4, and 1.6) nanostructures in the form of ribbons which has not been reported to date. For comparison, we have also included experimental data of the tetragonal $D0_{22}$-$Mn_{1.9}Ga$ sample.

EXPERIMENT

Mn_yGa ($y = 1.2$, 1.4, 1.6, and 1.9) nanostructured ribbons were prepared using arc-melting, melt-spinning, and annealing. The arc-melting process, which produces Mn_yGa ingots from the respective metal pieces, was carried out on a water-cooled Cu hearth in a highly pure argon environment. The Mn_yGa ingots were then inductively heated in a quartz tube and molten metal was ejected onto the surface of a rotating copper wheel where it rapidly solidified into ribbons. The ribbons are about 1 mm wide and 10 μm thick. The tangential speed of the rotating wheel was kept at 20 m/s for all the samples and the melt-spinning process was carried out in a chamber filled with a suitable pressure of high-purity argon gas. The ribbons were annealed in a tubular vacuum furnace with a base pressure $\sim 10^{-7}$ Torr at temperatures between

 © 2013 AIP Publishing LLC

[This article is copyrighted as indicated in the article. Reuse of AIP content is subject to the terms at: http://scitation.aip.org/termsconditions. Downloaded to] IP: 129.93.17.210 On: Thu, 19 Dec 2013 14:37:16

400 °C and 450 °C. $Mn_{1.2}Ga$ ribbons were annealed at 400 °C for 7 h and $Mn_{1.4}Ga$, $Mn_{1.6}Ga$, and $Mn_{1.9}Ga$ ribbons were annealed at 450 °C for 50 h to obtain the single-phase tetragonal structure. These annealing times are much shorter than the previously reported time of two to three weeks required for an arc-melted ingot to crystallize into a tetragonal phase.[17] The elemental compositions in the Mn_yGa alloys were estimated from the weights of the starting metal pieces and were later confirmed using energy-dispersive x-ray spectroscopy (EDS) on Joel JSM 840 A. The EDS values were very close to the initially estimated values within an error of 0.1 at. %. The room-temperature structural properties of the samples were studied using x-ray diffraction (XRD) in a Rigaku x-ray diffractometer and their microstructures were investigated using a FEI Tecnai Osiris Transmission Electron Microscope (TEM). A Quantum Design superconducting quantum interference device (SQUID) magnetometer and a Physical Properties Measurement System (PPMS) were used to investigate the magnetic and electron transport properties of the ribbons.

RESULTS AND DISCUSSION

Figure 1(a) shows the XRD patterns of Mn_yGa (y = 1.2, 1.4, and 1.6) ribbons measured at room temperature. All the diffraction peaks in the XRD patterns are indexed with the expected tetragonal $L1_0$-structure. However, as shown in the inset of Fig. 1(a), $Mn_{1.9}Ga$ ribbons annealed at 450 °C for 50 h crystallized in a different structure, the tetragonal $D0_{22}$ structure (c/a = 1.85). All the samples are polycrystalline but very small texture was observed in the ribbons. In order to understand the detailed crystal structure and to quantify the impurity phases, a Rietveld refinement of diffractograms of all the ribbon samples was carried out using the TOPAS software.[18] We also determined the *c* and *a*-axis lattice parameters from the Rietveld refinement of the XRD data (see Table I). Figure 1(b) shows a simulated powder diffraction pattern for tetragonal $Mn_{1.6}Ga$ alloy which is plotted with the experimental data. The intensities and 2θ positions of the diffraction peaks in the experimental pattern show a very close match with the simulated pattern indicating that the samples have crystallized in the tetragonal $L1_0$ structure. As all the Bragg reflections are accounted for by the $L1_0$ phase, we have not considered any secondary alloy phases and elemental impurities in the samples for Rietveld refinement. This suggests that the samples are single phase

TABLE I. Lattice parameters of Mn_yGa alloys.

Sample	$Mn_{1.2}Ga$	$Mn_{1.4}Ga$	$Mn_{1.6}Ga$	$Mn_{1.9}Ga$
c (Å)	3.720	3.661	3.633	7.239
a (Å)	3.873	3.882	3.893	3.918

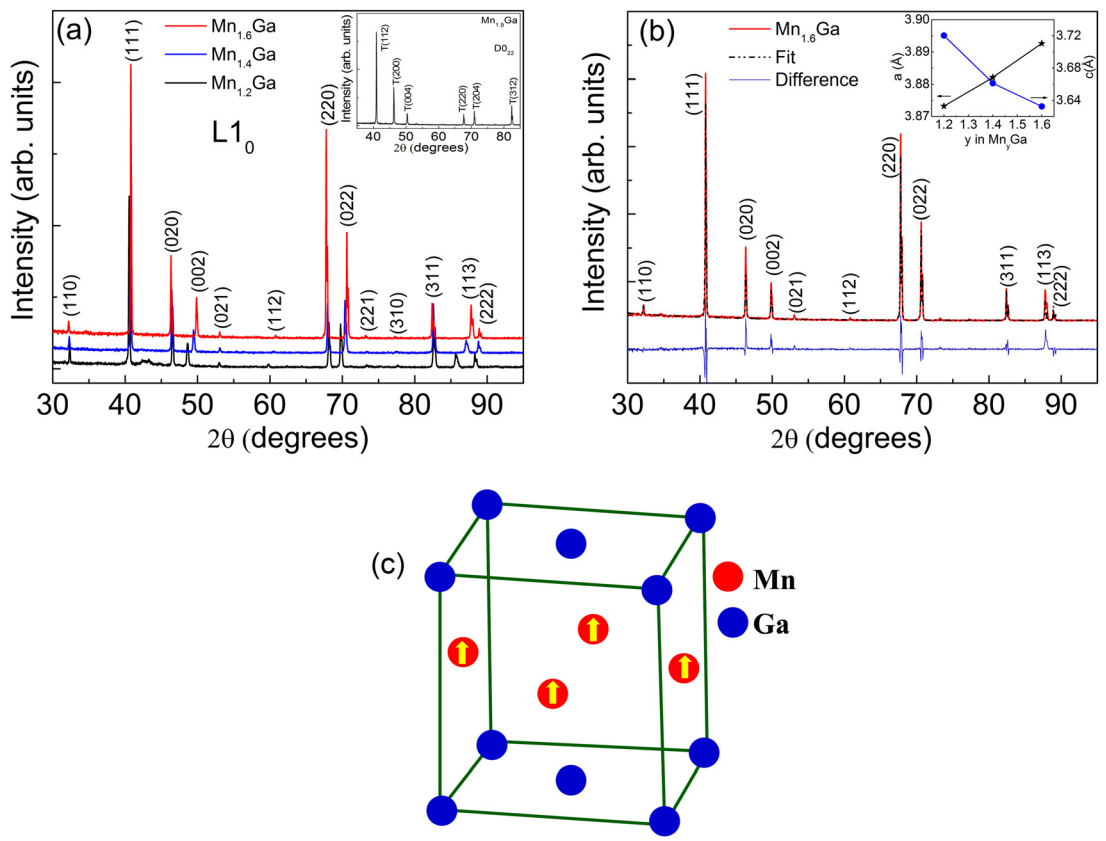

FIG. 1. (a) Room-temperature x-ray diffraction patterns of $Mn_{1.2}Ga$, $Mn_{1.4}Ga$, and $Mn_{1.6}Ga$ ribbons which are indexed to the tetragonal $L1_0$ structure. The inset shows an XRD pattern of $Mn_{1.9}Ga$ ribbon indexed to the tetragonal $D0_{22}$ structure. (b) A simulated powder x-ray diffraction pattern (Rietveld plot) corresponding to the tetragonal-$L1_0$ structure of $Mn_{1.6}Ga$ alloy with the experimental data (red line). The difference between the data and the fit is shown in blue color. The inset plots the lattice parameters *a* and *c* obtained from the Rietveld analysis of the XRD data as a function of y in Mn_yGa (y = 1.2, 1.4, and 1.6) alloy. (c) $L1_0$-MnGa unit cell.

[This article is copyrighted as indicated in the article. Reuse of AIP content is subject to the terms at: http://scitation.aip.org/termsconditions. Downloaded to] IP: 129.93.17.210 On: Thu, 19 Dec 2013 14:37:16

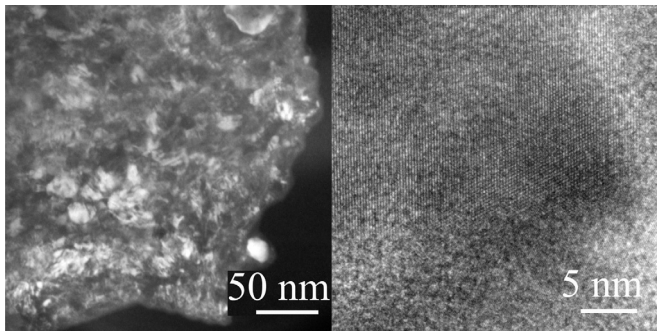

FIG. 2. TEM dark field image (left panel) and high resolution image (right panel) of a specimen prepared from the $Mn_{1.6}Ga$ ribbon.

Mn_yGa. As shown in the inset of Fig. 1(b) and Table I, both the *c* and *a*-axis lattice constants show a significant change with the change in Mn concentration in Mn_yGa. Although the change in *a* is small, the *c*-axis lattice parameter substantially decreases (approximately 2.4%) as y increases from 1.2 to 1.6. Such decrease of *c* with increasing y has also been observed in the bulk and thin film $L1_0$-Mn_yGa alloys.[19,20] Although the excess Mn atoms are believed to occupy some of the Ga sites causing a change in the lattice constants, the exact arrangement of these atoms in the $L1_0$ lattice is not known.[15] For Rietveld refinement, we also assumed statistical fractional occupation of Mn atoms at the Ga sites. Figure 1(c) shows the stoichiometric MnGa unit cell in $L1_0$ structure.

In order to determine the average particle size and to understand the microstructure of the ribbons, we have performed dark-field (DF) and high resolution TEM studies of one of the three samples, namely $Mn_{1.6}Ga$. The DFTEM image was taken with incident beam rotating along the peripheral of the selected diffraction rings so that all diffraction rings go through the object aperture. This allowed us to find more bright particles in the DFTEM image. As shown in the DFTEM micrograph (the left panel of Fig. 2), the specimen prepared from the $Mn_{1.6}Ga$ ribbon contains nanostructured particles with nonuniform size distribution and with many overlapping particles. The average particle size in the ribbon is about 35 nm ± 2 nm. The high-resolution TEM image (the right panel of Fig. 2) shows that the particles are single grained or have overlapping grains. The selected area diffraction (SAED) pattern was a ring pattern (not shown) confirming the polycrystalline nature of the sample. The crystal structure and lattice parameters determined from the TEM studies are consistent with the ones found from XRD analysis.

One of the interesting features of the Mn_yGa alloy is its tunable magnetic property. We have found that the magnetic properties including magnetization, coercivity, anisotropy energy, and Curie temperature of $L1_0$-Mn_xGa alloy are very sensitive to the alloy composition. Figure 3(a) shows the field-dependent magnetization of Mn_yGa ribbons measured at room temperature. All the samples show significant coercivities but the magnetizations are not saturated even at 70 kOe. This suggests that Mn_yGa ribbons have relatively large magnetic anisotropy as the polycrystalline samples of high anisotropy magnetic materials typically show such unsaturated M(H) loops. We have measured a high field (H = 70 kOe) magnetization as high as 621 emu/cm^3 in $Mn_{1.2}Ga$ ribbons which decreases almost linearly to 500 emu/cm^3 as y increases from 1.2 to 1.6. These values were calculated using the density (7.3 g/cm^3) of a stoichiometric MnGa alloy. The highest magnetization observed in our study (621 emu/cm^3) is smaller than the theoretically predicted value (845 emu/cm^3) for $L1_0$-MnGa alloy but is the highest experimental value for polycrystalline Mn_yGa compound reported to date. On the other hand, $Mn_{1.9}Ga$ ribbon which has $D0_{22}$ structure shows small magnetization of about 300 emu/cm^3 but the coercivity is slightly larger and is about 2.5 kOe. However, a high coercivity close to 10 kOe and M_r/M_s ratio more than 70% have been achieved after a magnetic field alignment of the powder samples prepared by a mechanical grinding of the ribbons (Fig. 3(a) inset). These values of magnetization and coercivity are comparable with the previously reported values for epitaxially grown $D0_{22}$-Mn_2Ga films.[11] The decrease of magnetization with increasing y in Mn_yGa ribbons suggests the possibility of having competing ferro- and antiferro-magnetic coupling in our samples. As mentioned above, we believe that the excess Mn atoms in the Mn_yGa ribbons may occupy some of the Ga

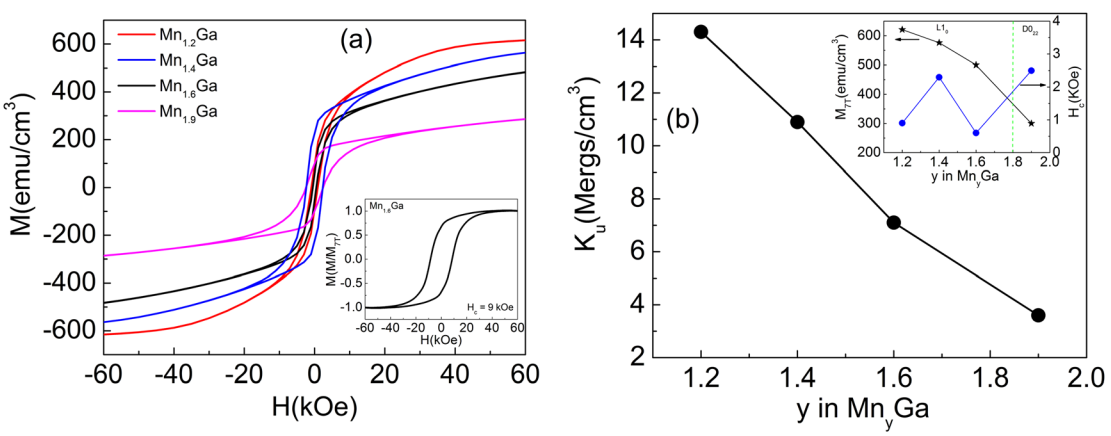

FIG. 3. (a) Room temperature magnetization as a function of magnetic field M(H) of Mn_yGa (y = 1.2, 1.4, 1.6, and 1.9) ribbons. Inset shows the M(H) hysteresis loop of a magnetic field aligned powder prepared from the $Mn_{1.6}Ga$ ribbon. (b) Magnetic anisotropy constant as a function of y in Mn_yGa. The inset of Fig. 3(b) shows how the high-field (H = 70 kOe) magnetization and coercivity change as the manganese concentration in Mn_yGa alloy changes.

[This article is copyrighted as indicated in the article. Reuse of AIP content is subject to the terms at: http://scitation.aip.org/termsconditions. Downloaded to] IP: 129.93.17.210 On: Thu, 19 Dec 2013 14:37:16

sites which couple antiferromagnetically with the Mn atoms in the regular $L1_0$ lattice. This is consistent with a theoretical prediction that the excess Mn atoms (δ) in $L1_0$-$Mn_{1+\delta}Ga$ occupy some of the Ga sites and couple antiferromagnetically with the rest of the Mn lattice.[15]

The anisotropy energy K_u, one of the most important properties of hard magnetic materials, was calculated using the approach-to-saturation method, where the high-field data were fitted to $M = M_0\ (1 - A/H^2) + \chi\ H$; $A = 4\,K^2/15\,M_0^2$. The parameters M_0, A, and χ are the spontaneous magnetization, a constant that depends on K and the high field susceptibility, respectively.[21] As shown in Fig. 3(b), K_u follows the trend of magnetization and decreases from 14 Mergs/cm^3 to 7 Mergs/cm^3 as y increases from 1.2 to 1.6. We note that the observed coercivity in our Mn_yGa ribbons does not scale with the anisotropy energy. Since coercivity is not an intrinsic magnetic property and also depends on the microstructure and texture of a sample, we do not expect the coercivity of the polycrystalline ribbons of a perpendicular anisotropy material to scale with their anisotropy energy.

The temperature dependence of magnetization for Mn_yGa (y = 1.2, 1.4, 1.6, and 1.9) ribbons is shown in Fig. 4. The magnetizations were measured at 1 kOe external field as the temperature increased from 300 K to 800 K. All the Mn_yGa samples show high ferromagnetic moments at room temperature but the magnetizations drastically decrease as the samples pass through their Curie temperatures (T_c). As shown in the inset of Fig. 4, all the samples show very high Curie temperatures, well above room temperature. The Curie temperatures of Mn_yGa ribbons show a strong composition dependence and increase almost linearly from 551 K to 702 K as y increases from 1.2 to 1.9. We note that $D0_{22}$-Mn_yGa nanostructures with y greater than 2.5 undergo structural phase transition before the Curie temperature is reached. But, interestingly, the structural and magnetic transitions are decoupled for $D0_{22}$-Mn_yGa with $y \leq 2.1$.[13] This is true for $L1_0$-Mn_yGa nanostructures as well and the measured phase-transition temperatures correspond to the real Curie temperatures.

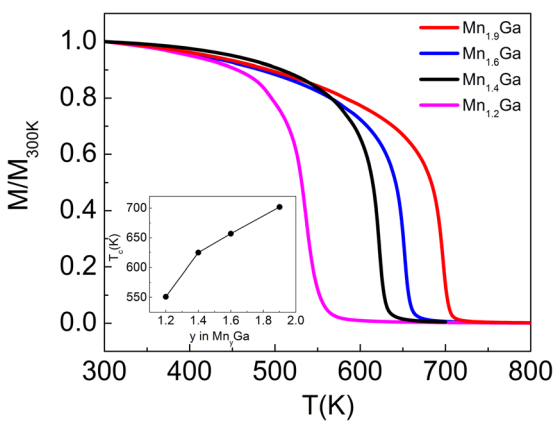

FIG. 4. Normalized magnetization ($M/M_{300\,K}$) as a function of temperature of Mn_yGa (y = 1.2, 1.4, 1.6, and 1.9) ribbons measured at H = 1 kOe during heating from room temperature to 800 K. The inset plots the Curie temperature as a function of y.

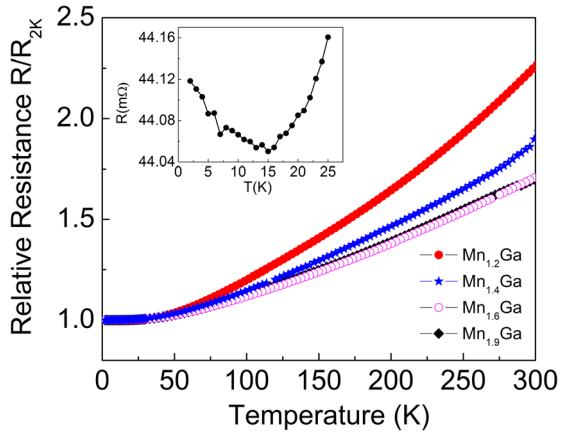

FIG. 5. Relative resistance ($R/R_{2\,K}$) as a function of temperature of Mn_yGa (y = 1.2, 1.4, 1.6, and 1.9) ribbons. Inset shows the expanded view of the low-temperature (between 2 K and 25 K) R(T) curve of $Mn_{1.2}Ga$ ribbon.

The electrical resistances of Mn_yGa ribbons were measured as a function of temperature between 2 K and 300 K using a four-point-probe method. The data were recorded during cooling from 300 K to 2 K. As shown in Fig. 5, the resistances are normalized to the value at 2 K for better comparison. All the samples are highly conducting and show typical metallic behavior where the resistances increase as temperature increases. The residual resistances are in the range of tens of milliohms (resistivity at 2 K $\sim 2 \times 10^{-4}\,\Omega$ cm for $Mn_{1.2}Ga$). The low temperature resistances of Mn_yGa samples with y = 1.4, 1.6, and 1.9 are almost constant but the sample with y = 1.2 shows a resistance minimum followed by a small upturn below the minimum. Such resistivity minima have also been observed in Mn_yGa films and are attributed to the structural disorder and grain boundary scattering.[22] The suppression of resistivity minima in samples having higher Mn concentrations may have been caused by their higher residual resistances. The residual resistance ratio (RRR) defined as $R_{300\,K}/R_{2\,K}$ is 2.3 for $Mn_{1.2}Ga$ which decreases with increasing Mn concentration and reaches 1.7 for $Mn_{1.6}Ga$. These values are very close to those reported for high quality epitaxial films grown on GaN (0001) layer using molecular beam epitaxy.[22] The decrease in the RRR with increasing Mn concentration can be attributed to the structural disorder caused by a partial occupation of some of the Ga sites by the excess Mn atoms.

CONCLUSIONS

In summary, the structural, magnetic, and electron-transport properties of single phase Mn_yGa (y = 1.2, 1.4, 1.6, and 1.9) ribbons prepared by arc melting, melt spinning, and annealing have been investigated. X-ray diffraction showed that the Mn_yGa ribbons with y = 1.2, 1.4, and 1.6 crystallize in the tetragonal $L1_0$ structure whereas the sample with y = 1.9 crystallizes in the tetragonal $D0_{22}$ structure. The magnetic properties of the samples were found to be very sensitive to the elemental composition of Mn_yGa alloy where the magnetization and anisotropy energy decrease and Curie temperature increases with increasing y. All the ribbons showed metallic electron transport between 2 K and 300 K but the

[This article is copyrighted as indicated in the article. Reuse of AIP content is subject to the terms at: http://scitation.aip.org/termsconditions. Downloaded to] IP: 129.93.17.210 On: Thu, 19 Dec 2013 14:37:16

$Mn_{1.2}Ga$ also showed a resistance minimum near 15 K. The observed magnetic properties are consistent with a ferromagnetic structure in the perfectly ordered $L1_0$-MnGa lattice plus an antiferromagnetic coupling with antisite Mn atoms.

ACKNOWLEDGMENTS

This research was supported by DOE (DE-F602-04ER46152) (DJS, RS), NSF MRSEC (NSF-DMR-0820521) (PK, YH), NSF MRI TEM (DMR-0960110) and NCMN (VRS, XZL). We would like to thank J. E. Shield for using his sample preparation facility.

[1]C. Chappert, A. Fert, and F. N. Van Dau, Nature Mater. **6**, 813 (2007).
[2]R. Sbiaa, H. Meng, and S. N. Piramanayagam, Phys. Status Solidi (RRL) **5**, 413 (2011).
[3]R. Skomski and J. M. D. Coey, *Permanent Magnetism* (Institute of Physics Publishing, Bristol, 1998).
[4]N. Poudyal and J. P. Liu, J. Phys. D: Appl. Phys. **46**, 043001 (2013).
[5]P. Kharel, V. R. Shah, X. Z. Li, W. Y. Zhang, R. Skomski, J. E. Shield, and D. J. Sellmyer, J. Phys. D: Appl. Phys. **46**, 095003 (2013).
[6]J. B. Yang, Y. B. Yang, X. G. Chen, X. B. Ma, J. Z. Han, Y. C. Yang, S. Guo, A. R. Yan, Q. Z. Huang, M. M. Wu, and D. F. Chen, Appl. Phys. Lett. **99**, 082505 (2011).
[7]D. P. Hoydick, E. J. Palmiere, and W. A. Soffa, J. Appl. Phys. **81**, 5624 (1997).
[8]T. Saito and R. Nishimura, J. Appl. Phys. **112**, 083901 (2012).
[9]L. Zhu, S. Nie, K. Meng, D. Pan, J. Zhao, and H. Zheng, Adv. Mater. **24**, 4547 (2012).
[10]F. Wu, S. Mizukami, D. Watanabe, H. Naganuma, M. Oogane, Y. Ando, and T. Miyazaki, Appl. Phys. Lett. **94**, 122503 (2009).
[11]H. Kurt, K. Rode, M. Venkatesan, P. Stamenov, and J. M. D. Coey, Phys. Status Solidi B **248**, 2338 (2011).
[12]K. M. Krishnan, Appl. Phys. Lett. **61**, 2365 (1992).
[13]Y. Huh, P. Kharel, V. R. Shah, E. Krage, R. Skomski, J. E. Shield, and D. J. Sellmyer, "Magnetic and Structural Properties of Rapidly Quenched Tetragonal $Mn_{3-x}Ga$ Nanostructures," IEEE Trans. Magn. **49**(7) (in press).
[14]S. Wurmehl, H. C. Kandpal, G. H. Fecher, and C. Felser, J. Phys.: Condens. Matter **18**, 6171 (2006).
[15]A. Sakuma, J. Magn. Magn. Mater. **187**, 105 (1998).
[16]L. Zhu and J. Zhao, Appl. Phys. A **111**, 379–387 (2013).
[17]J. Winterlik, B. Balke, G. H. Fecher, C. Felser, M. C. M. Alves, F. Bernardi, and J. Morais, Phys. Rev. B **77**, 054406 (2008).
[18]TOPAS-V 4.2, Bruker AXS, Inc.
[19]H. Niida, T. Hori, H. Onodera, Y. Yamaguchi, and Y. Nakagawa, J. Appl. Phys. **79**, 5946 (1996).
[20]S. Mizukami, T. Kubota, F. Wu, X. Zhang, T. Miyazaki, H. Naganuma, M. Oogane, A. Sakuma, and Y. Ando, Phys. Rev. B **85**, 014416 (2012).
[21]G. Hadjipanayis and D. J. Sellmyer, Phys. Rev. B **23**, 3349 (1981).
[22]A. Bedoya-Pinto, C. Zube, J. Malindretos, A. Urban, and A. Rizzi, Phys. Rev. B **84**, 104424 (2011).

[This article is copyrighted as indicated in the article. Reuse of AIP content is subject to the terms at: http://scitation.aip.org/termsconditions. Downloaded to] IP: 129.93.17.210 On: Thu, 19 Dec 2013 14:37:16